nature materials

ARTICLES

PUBLISHED ONLINE: 14 AUGUST 2011 | DOI: 10.1038/NMAT3089

Probing bulk electronic structure with hard X-ray angle-resolved photoemission

A. X. Gray[1,2]*, C. Papp[1,2,3], S. Ueda[4], B. Balke[1,2,5], Y. Yamashita[4], L. Plucinski[6], J. Minár[7], J. Braun[7], E. R. Ylvisaker[1], C. M. Schneider[6], W. E. Pickett[1], H. Ebert[7], K. Kobayashi[4] and C. S. Fadley[1,2]

Traditional ultraviolet/soft X-ray angle-resolved photoemission spectroscopy (ARPES) may in some cases be too strongly influenced by surface effects to be a useful probe of bulk electronic structure. Going to hard X-ray photon energies and thus larger electron inelastic mean-free paths should provide a more accurate picture of bulk electronic structure. We present experimental data for hard X-ray ARPES (HARPES) at energies of 3.2 and 6.0 keV. The systems discussed are W, as a model transition-metal system to illustrate basic principles, and GaAs, as a technologically-relevant material to illustrate the potential broad applicability of this new technique. We have investigated the effects of photon wave vector on wave vector conservation, and assessed methods for the removal of phonon-associated smearing of features and photoelectron diffraction effects. The experimental results are compared to free-electron final-state model calculations and to more precise one-step photoemission theory including matrix element effects.

The use of angle-resolved photoemission spectroscopy (ARPES) to determine the electronic structure of materials is a much-used technique with many successes[1–3]. The electronic structure of a host of materials of fundamental interest, from prototypical transition metals such as W (refs 4–6), to more complex and technologically relevant substances, such as future semiconductors or topological compounds[7,8], or strongly correlated materials[3,9], have been successfully studied in the past. However, the inherent surface sensitivity of conventional ARPES, due to the low inelastic mean-free paths (IMFPs) of the photoemitted electrons, with kinetic energies usually ranging between about 20 and 150 eV, can lead to spectra that are strongly influenced by surface effects. This can of course be of great advantage in the description of new materials and their surfaces. Conversely, this surface sensitivity can become a major disadvantage if the bulk properties of the materials studied are of particular interest or significantly different from the surface properties, or if it is difficult to prepare a sufficiently good surface for standard ARPES measurements.

This surface sensitivity has led recently to several studies in which ARPES has been carried out with photon energies up to the 1 keV range[10–13]. These studies for a variety of systems, but especially for several strongly correlated materials, have shown the advantage of probing more deeply below the surface. One can thus also immediately ask whether going further into the multi-keV hard X-ray regime might also be possible and useful in this regard[14,15].

The recent advent of new high-energy third-generation synchrotron facilities and the development of new high-energy electron analysers make it possible to attempt such novel angle-resolved experiments in the hard X-ray regime. The overall energy resolutions (down to ∼50 meV), as well as the angular resolutions of these newly developed facilities (down to ∼0.2°–0.3°), in principle make it possible to meaningfully study dispersive energy bands at up to, for example, 3–6 keV excitation energies, and with wave vector resolutions of 0.1–0.2 Å^{-1}. Going to multi-keV energies increases the inelastic mean-free path of the electrons roughly as [kinetic energy]$^{0.75}$ (refs 16–18), and thus by a factor of about 10–20 from typical ARPES studies, going from about 5 Å to about 50–100 Å, thereby markedly enhancing the bulk sensitivity of the measurement, and also in principle permitting the study of deeply buried layers.

However, a few additional considerations are involved in measuring and interpreting such hard X-ray angle-resolved photoemission (HARPES) data[14]. First, it is well known that the creation and annihilation of phonons in the photoexcitation process can smear out the specification of $\mathbf{k}_i$, the initial-state wave vector[6,14,19]. An approximate way of estimating the effect of this is to calculate a photoemission Debye–Waller factor from $W(T) = \exp[-(1/3)g_{hk\ell}{}^2\langle U^2(T)\rangle]$, where $g_{hk\ell}$ is the magnitude of the bulk reciprocal lattice vector involved in the direct transitions at a given photon energy and $\langle U^2(T)\rangle$ is the three-dimensional mean-squared vibrational displacement[6,14,19]. With $W(T) \gtrsim 90\%$, one is in the **k**-resolving or ultraviolet photoelectron spectroscopy (UPS) limit. With $W(T) \lesssim 10\%$, one is in the density-of-states or X-ray photoelectron spectroscopy (XPS) limit. In addition, deviations from the dipole approximation for excitation lead to the inclusion of the photon momentum in the simplest form of the wave vector conservation equation:

$$\mathbf{k}_i = [\mathbf{k}_f - \mathbf{k}_{h\nu}] - g_{hk\ell} \quad (1)$$

where $\mathbf{k}_i$ is the initial-state wave vector in the reduced Brillouin zone (BZ), $\mathbf{k}_f$ is the final-state wave vector inside the crystal, after allowing for the crossing of the inner potential, and $\mathbf{k}_{h\nu}$ is the wave vector of the photon[6,11–14]. As $\mathbf{k}_f$ is a much longer

[1]Department of Physics, University of California Davis, Davis, California 95616, USA, [2]Materials Sciences Division, Lawrence Berkeley National Laboratory, Berkeley, California 94720, USA, [3]Lehrstuhl für Physikalische Chemie II, Universität Erlangen-Nürnberg, 91058 Erlangen, Germany, [4]NIMS Beamline Station at SPring-8, National Institute for Materials Science, Hyogo 679-5148, Japan, [5]Institut für Anorganische und Analytische Chemie, Johannes Gutenberg-Universität, 55099 Mainz, Germany, [6]Peter Grünberg Institut PGI-6, Research Center Jülich, 52425 Jülich, Germany, [7]Department of Chemistry, Ludwig Maximillian University, 81377 Munich, Germany. *e-mail: agray@ucdavis.edu.

vector in HARPES, with $|\mathbf{k}_f| \propto [\text{kinetic energy}]^{1/2}$, the angular precision in setting up and interpreting an experiment becomes more critical, as we discuss below. Recoil effects due to momentum conservation will also induce a broadening and shifting of spectral features in energy[20], even if these were negligible for the systems studied here; the recoil shifts are estimated to be 18 meV for W and 23 meV for GaAs. Finally, as in all ARPES measurements, the relative intensities of various features will depend on the specific matrix elements involved, with these in turn depending roughly on the weighted atomic cross-sections contributing to each band, as well as on the overall symmetry of the experimental geometry. Cross-section arguments, for example, imply that *d*- and *f*-character will be strongly suppressed as the energy is increased, with *s*- and *p*-character gaining in importance[12,15]. Although the latter are more important in general with respect to transport properties, learning something about the former thus has to be more indirect, through *d*- and *f*-hybridization with *s*- and *p*-states[2].

As a first system to be studied using HARPES, we choose single-crystal W with the (110) orientation, which is well-understood from the theoretical and experimental points of view, thus allowing for an easy comparison to earlier results[4–6,12,13,21,22]. Furthermore, W is well-suited to such high-energy experiments because of its high Debye temperature and high atomic weight, leading to high Debye–Waller factors with cryogenic cooling[6]. For 6 keV excitation of the valence electrons of W, this factor is about 0.45 at 30 K, and about 0.09 at 300 K, so measuring at these two temperatures spans a range from about 45% direct transitions (roughly halfway between UPS and XPS limits) to about 9% direct transitions (essentially in the XPS limit). We can also estimate the average probing depth in our experiment using optical properties or the widely-used TPP-2M formula[16–18], which yields an IMFP of 56–61 Å for the W valence electrons at the photon energy of 6 keV which we will use. These values are about 13 times larger than the IMFP for 100 eV-electrons and about 42 times larger than that for 20 eV-electrons. They also correspond to an average emission depth that is 18–19 W unit cells, using $a = 3.16$ Å as the unit-cell dimension. Thus, we expect to probe bulk properties much more clearly at 6 keV than is possible with the typical energies of previous ARPES experiments.

The second system we have investigated using HARPES is the semiconductor GaAs in the (001) orientation, a material that is widely used in solar cells, light-emitting diodes and laser diodes, and, owing to its high electron mobility, finds a multitude of applications in fast-switching electronic devices. GaAs may also have future applications in high-efficiency solar-cell technology and spintronic devices[23–28]. The lower Debye temperature and effective atomic mass of GaAs suggests working at lower photon energies. Our measurements were thus performed on GaAs with an excitation energy of 3.2 keV, at which the relevant Debye–Waller factors are 0.31 at 20 K and 0.01 at 300 K. At this photon energy, the inelastic mean-free path for GaAs valence electrons is predicted by TPP-2M to be 57 Å, and recently measured to be about 32 Å(ref. 29), values which are expected to be about 11 times larger than the value at 100 eV, and about 38 times larger than the value at 20 eV. Thus, at 3.2 keV, and using $a = 5.65$ Å as the lattice constant for GaAs, we should have the ability to probe, on average, 6–10 unit cells into the sample, and our measurements should again become more truly bulk-sensitive. All of our measurements were carried out at the SPring-8 facility in Japan; further experimental details are contained in the Methods section below.

Figure 1 shows HARPES spectra of W(110) taken at a photon energy of 5,956 eV, together with corresponding theoretical calculations. These data represent single detector images spanning approximately 12°, as indicated in Fig. 1e. Differences between the measurements shown in Fig. 1a at room temperature and Fig. 1b at 30 K clearly illustrate the strong effect of temperature. The spectra in Fig. 1a show a clear, but non-dispersive, modulation in angle of energy-distribution curves that are found to be essentially identical in form and very similar to the total density of states (DOS) for W (see for example ref. 21); these modulations can be attributed to core-like X-ray photoelectron diffraction (XPD; ref. 30 and references therein), whereas the spectra at lower temperature (Fig. 1b) already show clear signs of the dispersive W bands. However, the low-temperature HARPES image still contains a component modulated in energy by the DOS, as derived from the angular average of the room-temperature data in Fig. 1a and shown as the yellow curve on the same figure, and by XPD in angle, as derived from the energy-averaged grey contour in Fig. 1a. By applying a two-step normalization procedure to the low-temperature data in Fig. 1b using the averaged room-temperature contours, in which there is first a division by the yellow curve and then by the grey curve (A. Bostwick and E. Rotenberg, private communication) we can correct in some way for both DOS- and XPD-like effects in the data, and indeed the dispersing bands are much more clearly seen in the corrected Fig. 1c. Such a procedure results in minor shifts of the features in energy and momentum, with the magnitude of these shifts increasing as the derivative of the normalization profiles.

The dispersive valence-band features in Fig. 1c are repeated about three times over the entire detector image. This quasi-periodicity can be understood with the help of an extended-zone scheme, as shown in Fig. 1f, where all vectors are shown to scale. The extended-zone scheme permits an easily visualizable analysis of the data using a free-electron final-state model and the basic wave vector conservation theory given by equation (1). For W, the primitive cell dimension is given by $2\pi/a = 1.988$ Å^{-1}. The magnitude of the final-state photoelectron wave vector inside the crystal, after allowing for an inner potential of 15 eV for W, a work function of 4.5 eV, and an average valence binding energy of about 4 eV, is given by $|\mathbf{k}_f|(\text{Å}^{-1}) = 0.512\bar{E}_{kin,i}^{0.5}\,(\text{eV}) = 39.53$ Å^{-1} $= (19.88)2\pi/a$, where $\bar{E}_{kin,i}$ is the average kinetic energy inside the surface relative to the valence band minimum. The magnitude of the photon momentum can be calculated using $|\mathbf{k}_{h\nu}|(\text{Å}^{-1}) = 0.000507\,h\nu(\text{eV}) = 3.01 = (1.51)2\pi/a$. With the 90° angle between photon incidence and electron emission, the magnitude of the final-state photoelectron wave vector as adjusted for the photon momentum is thus given by

$$\begin{aligned} |\mathbf{k}_f - \mathbf{k}_{h\nu}| &= (39.53^2 + 3.01^2)^{1/2} = 39.64\ \text{Å}^{-1} \\ &= 14.10\sqrt{2}(2\pi/a) = 19.94(2\pi/a) \end{aligned}$$

Figure 1f now shows the vectors involved in an extended zone picture, with the sector of the red circle corresponding to the arc traversed by $[\mathbf{k}_f - \mathbf{k}_{h\nu}]$, and thus also by $\mathbf{k}_i$ in the reduced BZ. Also indicated is the single *g*-vector involved in our data, which has a magnitude of $14\sqrt{2}(2\pi/a) = 19.80(2\pi/a)$, leading to a measurement that passes virtually through the N point of the BZ. Furthermore, the large diameter of $[\mathbf{k}_f - \mathbf{k}_{h\nu}]$ implies that scanning the angle near normal should essentially move the sampling point along a nearly straight line, thus sampling repeated N–Γ–N regions. This repeated pattern is, in fact, seen in the experiment, with a repeat distance of about 4.1°, which is very close to the 4.21° N–Γ–N angular distance expected from the extended-zone picture.

Also shown in Fig. 1c as green curves are the results of theoretical calculations based on a simple model which couples the W band structure (as calculated with the Wien2k program[31]) with free-electron final-states using equation (1), and there is in general very good agreement with experiment as to the features and bands expected, although of course there is no information in these curves as to relative intensities, as no allowance is made for matrix elements. Of note is that experiment shows more structure than the free-electron final-state theory over about 1–2 eV in binding energy (for example feature labelled 4), but this could be the result

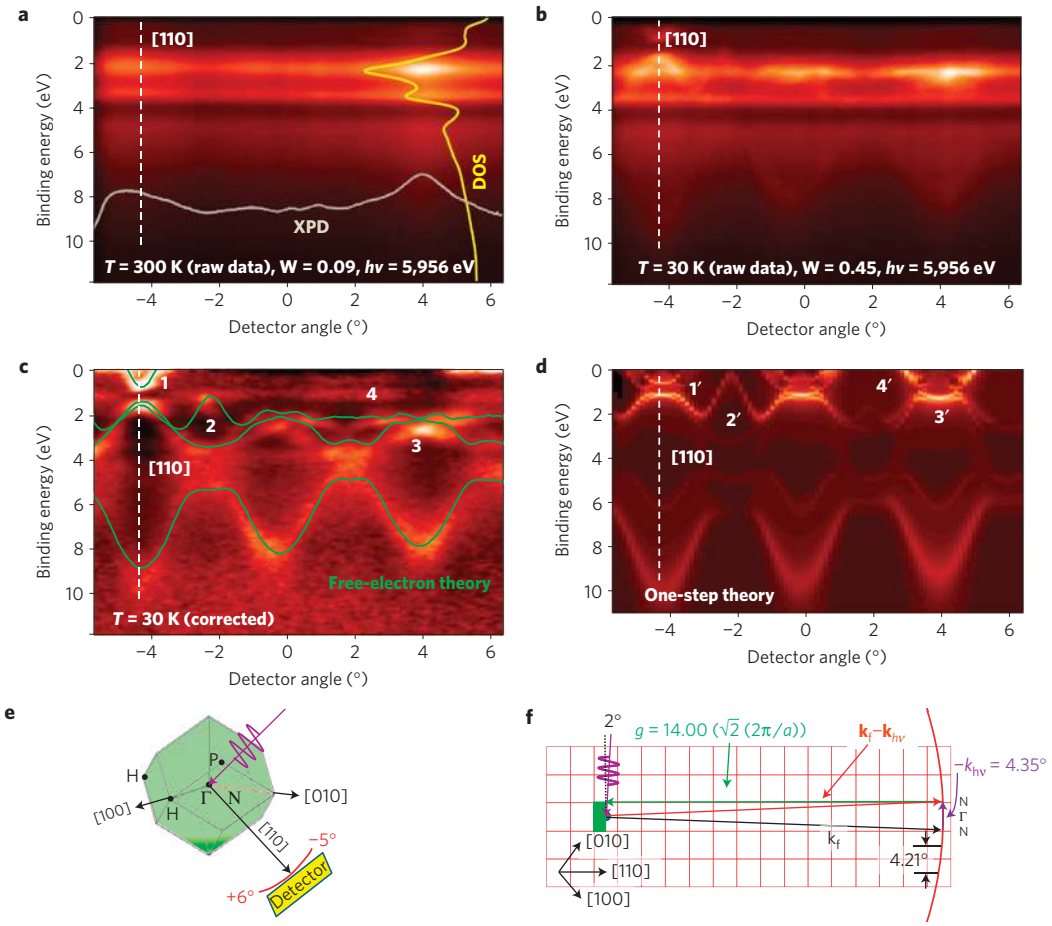

Figure 1 | Hard X-ray angle-resolved photoemission (HARPES) measurements and theory for W(110) at a photon energy of 5,956 eV. a, Room temperature HARPES measurement from W(110). The spectra are dominated by modulations due to the DOS in energy (yellow curve) and XPD effects in angle (grey curve). Dispersive features are not observed owing to the low fraction of direct transitions at room temperature in this hard X-ray regime. The Debye–Waller factor here is only 0.09. **b**, The same measurement as in **a**, but at 30 K. Phonon effects are suppressed at low temperature and dispersive features are now apparent. The Debye–Waller factor here is 0.45. **c**, Data from **b**, normalized by means of a 2-step process so as to remove the DOS and XPD effects (yellow and grey curves in **a**), thus enhancing dispersive valence-band features. The solid curves superimposed on the experimental data are the results of band-structure-to-free-electron final-state model calculations. Some prominent features 1–4 are labelled. A sample misalignment of 0.5° toward [001] was used in the free-electron final-state calculation, as the value which produces the best fit between the experiment and theory. **d**, One-step photoemission calculations of the HARPES spectra taking into account matrix-element effects. Corresponding features 1′-4′ are labelled. **e**, The experimental geometry relative to the first BZ. **f**, An extended BZ picture of the HARPES measurement for W.

of experimental **k** smearing due to inelastic scattering and finite angular resolution, which allows more initial states to contribute than are allowed in the free-electron or one-step models (see Supplementary Discussion).

Finally, in Fig. 1d we show the results of much more accurate one-step theory based on a local density approximation (LDA) layer-KKR (Korringa–Kohn–Rostoker) approach with a time-reversed LEED (low-energy electron diffraction) final-state[32] over the same range in angle (see Supplementary Discussion). The resemblance of the data in Fig. 1c to the one-step theory in Fig. 1d is indeed remarkable, with features labelled 1, 2, and 3, and the weaker 4 in experiment being correctly modelled by features 1′, 2′, 3′ and 4′ in theory. The effect of the photon momentum $\mathbf{k}_{h\nu}$, is to shift $[\mathbf{k}_f - \mathbf{k}_{h\nu}]$ relative to $\mathbf{k}_f$ by 4.35°, which by coincidence moves it almost exactly the N–Γ–N distance of 4.21° (see extended zone image in Fig. 1f).

Other minor discrepancies observed between the experimental band structure and the theoretical calculations can easily arise owing to a slightly misaligned sample. For our geometry, this misalignment or tilt is defined as the deviation of the electron analyser lens axis from the [110] direction. Unlike in conventional low-energy ARPES, for HARPES even a small sample tilt (0.5°–1.0°) results in a significant impact on the spectra, with these at least qualitatively predicting effects in the direction observed (see Supplementary Discussion). Such misalignment was in fact allowed for in the free-electron final-state calculation (Fig. 1c) by introducing the tilt angle of 0.5° toward the [001] direction, the value which produces the best fit between the experiment and theory. Allowing for such a tilt in the one-step theory is at present prohibitively difficult from a computational point of view (see Supplementary Discussion).

These first HARPES measurements on a prototypical transition metal thus provide a clear picture of the possibilities and challenges of HARPES. There is a need for cryogenic cooling and appropriate data treatment, including some kind of correction for both phonon-produced DOS-like features and XPD-like features. Using these results from W as a measure for the feasibility of HARPES measurements in general, we would conclude as a first conservative estimate that a Debye–Waller factor of about 0.45 or greater is required to obtain a sufficient fraction of direct transitions.

Measurements were also performed on a semi-insulating GaAs (001) sample, cut from a liquid-encapsulated Czochralski grown

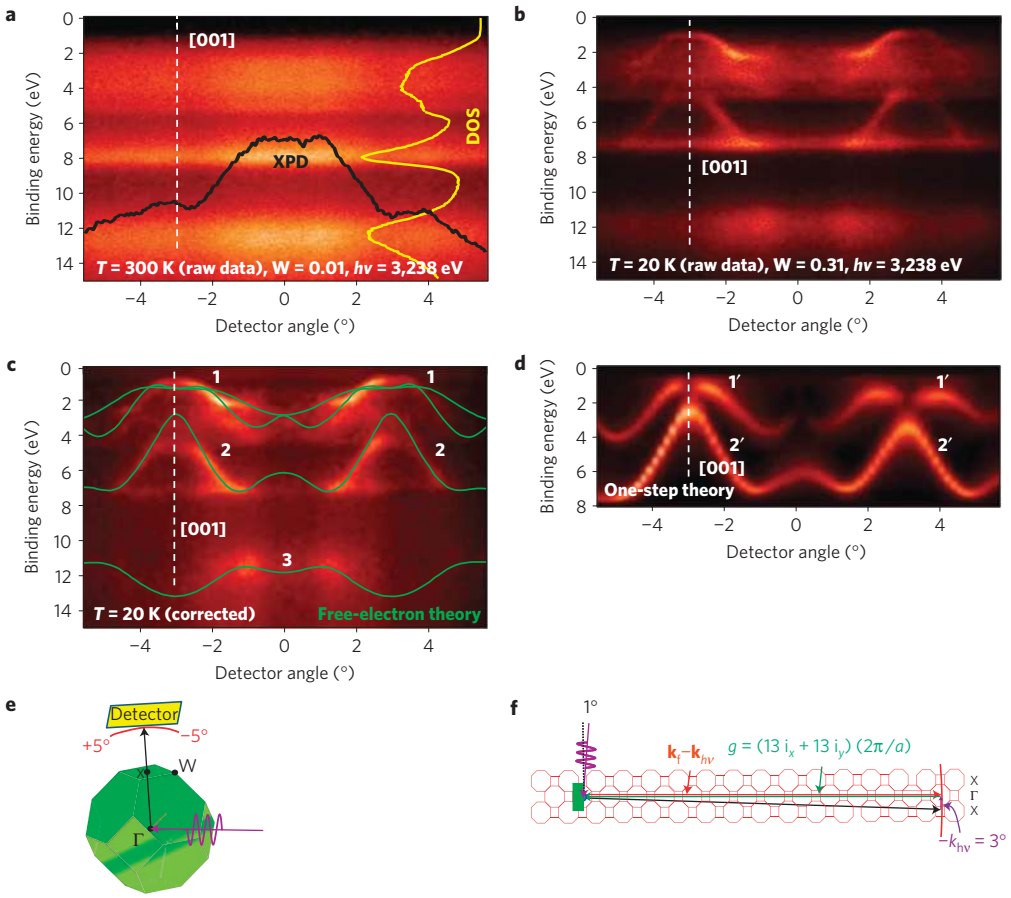

Figure 2 | HARPES measurements and theory for GaAs(001) at a photon energy of 3,238 eV. a, Room temperature measurement from GaAs(001), with a Debye–Waller factor 0.01 and average curves representing DOS and XPD again shown. **b**, The same measurement as in **a**, but at 20 K, with a Debye–Waller factor of 0.31. **c**, Same measurement, corrected so as to remove the DOS and XPD effects. The solid curves superposed on the experimental data are the results of the free-electron final-state calculations. Prominent features 1–3 are labelled. **d**, One-step photoemission calculations of the HARPES spectra, taking into account matrix-element effects, with corresponding features 1′–3′ labelled. The theoretical results in both **c** and **d** are calculated for the ideal geometry, with no tilt included. **e**, The experimental geometry relative to the first BZ. **f**, An extended BZ picture of the HARPES measurement for GaAs.

GaAs wafer that was lightly p-doped with As anti-site defects to pin the Fermi level approximately in the middle of the band gap (see details in Supplementary Discussion). GaAs has a lower average atomic mass and Debye temperature than W, and thus smaller photoemission Debye–Waller factors, so it was studied with a photon energy of 3,238 eV and sample temperatures of 20 K and 300 K; the results are summarized in Fig. 2 in the same format as Fig. 1. Under these conditions, the Debye–Waller factors are smaller, 0.31 for 20 K and 0.01 for 300 K, so we expect DOS- and XPD-like effects to be stronger in the raw data, even at low temperature. Nonetheless, the raw low-temperature data in Fig. 2b clearly show dispersing bands over about 0–8 eV binding energy, and they are even clearer in the raw data than those for W, with a Debye–Waller factor of 0.45, indicating a potentially beneficial material dependence in phonon broadening that requires a better theoretical explanation. These features are also seen in the data in Fig. 2c that have had the two-step DOS + XPD correction applied to them; here, these corrections are not as critical, and may even suppress some features. Again, in Fig. 2c the positions of the allowed direct transitions based on the free-electron model are shown, and there is in general very good agreement, with the exception of the band labelled 3 at about 12 eV binding energy, to which we return below. Figure 2d further shows the results of one-step theoretical calculations, and there is again very good agreement with experiment in Fig. 2b,c. However, one discrepancy worth discussing concerns the separations between bands 1 and 2 and 1′ and 2′, which are less than those in the experiment for both types of theoretical modelling. This disagreement could be due to a small tilt of the sample from the ideal geometry, as well as additional $\mathbf{k}$ smearing due to inelastic scattering and finite angular resolution, or many-electron effects not included in either theoretical treatment (see Supplementary Discussion).

It is worth noting here that some band bending near the surface of this sample might be present, but from the semi-insulating nature of the sample and the low carrier concentrations, we expect this to extend much deeper than the IMFP for photoelectrons in GaAs (see Supplementary Discussion). Thus, beyond some rigid shift of features that we do not expect to be greater than 0.5 eV, band bending should not affect our results.

In the extended-zone picture of the GaAs data, the reciprocal-space picture is slightly more complicated than that for W, owing to the different stacking of the BZs (Fig. 2f). This drawing again allows us to estimate the locus of points probed in the BZ. Here, $|\mathbf{k}_f - \mathbf{k}_{hv}|$ is 13.13 $(4\pi/a)$, leading to a g vector of 13 $(4\pi/a)$, and again a central $\mathbf{k}_i$ point close to the Γ point. The angular distance between the two spectral features in Fig. 2a,b is 6.2°, which corresponds to twice the distance from Γ to K to X in the extended-zone scheme. Good agreement between the experimental data and earlier linear muffin-tin orbital-type band-structure calculations also confirms the region in the BZ being sampled in this HARPES experiment[33].

The only significant difference between theory and experiment lies in the lack of dispersion of the band at 12 eV. Band structure

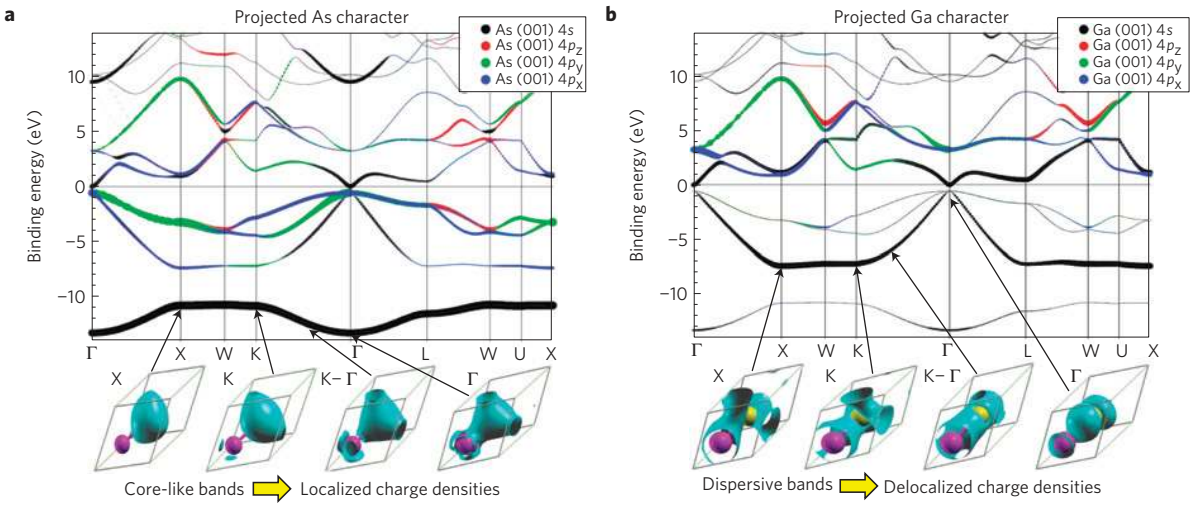

Figure 3 | First-principles local density calculations of the GaAs band structure. GaAs band structure projected onto the As (**a**) and Ga (**b**) atomic orbital makeup, with curve widths indicating the relative strengths of each contribution, together with corresponding charge density contours at various symmetry points for the lowest two bands.

calculations show a dispersion of about 2 eV (see Figs 2c and 3), but the measurement only has a variation with angle in intensity in this region, suggesting more core-like XPD behaviour. In fact, the XPD profile for room-temperature XPS shown in Fig. 2a is very close to that observed for this band in Fig. 2b. A likely explanation for this behaviour is a strong spatial localization of this particular band on As over the entire BZ, as shown in Fig. 3 through projected band structures illustrating the atomic orbital makeup of each band for both As and Ga, as well as total charge density contours for this band and the one just above it. These results indicate that the electrons in the band at 12 eV behave more like localized core states, which should have stronger electron–phonon coupling and thus converge to a DOS/XPD type of behaviour more quickly than the bands above them, which are much more delocalized.

We have demonstrated that angle-resolved photoemission is possible with high-energy X-rays in the multi-keV regime, thus allowing for more bulk-sensitive electronic structure determinations. Insight into the relevant physics is provided by both simple free-electron final-state modelling together with ground-state band structures, and state-of-the-art one-step photoemission theory including matrix elements. These first-time measurements thus open new possibilities in the field of materials science because of the unique advantages of bulk-sensitivity, and of using samples 'as prepared' because of the low surface sensitivity. In addition to this, this new technique opens the possibility of mapping the entire BZ, either by rotating the spectrometer with respect to the sample so as to acquire several segments of the $[\mathbf{k}_f - \mathbf{k}_{h\nu}]$ arc at one photon energy and then mapping these into a single BZ (see Figs 1f and 2f), or more simply by varying the photon energy with a fixed spectrometer orientation. Studies of buried layers in multilayer structures should also be possible, for example if a metallic layer is situated underneath an insulator such that the metallic bands can be seen through the insulator bandgap. Of course, the energy resolutions in HARPES, which were here about 250 meV, but in the future clearly can go to 50 meV, if not smaller, will not reach the 1 meV or smaller of conventional ARPES. Also, recoil effects will be more pronounced for materials containing lighter atoms. Resolution in $\mathbf{k}_f$, and thus also $\mathbf{k}_i$, will ultimately be limited by the lens characteristics, but as a smaller angular range is needed to span the Brillouin zone (BZ) in one direction in HARPES (for example, only 4.1° for W(110) at 6 keV and 6.2° for GaAs(001) at 3.2 keV), a smaller cone angle could be used in HARPES, with this making it easier for the electron optics to achieve higher angular resolution. We also expect that the theoretical treatment of phonon effects will improve, and it is clear from our results that the simple approach of using a Debye–Waller factor to estimate the degree of phonon involvement has limitations, with GaAs being more amenable to study than might be expected on this basis. Such improved theory should also lead to better data-correction procedures, and the analysis of the direct-transition aspects will thus become more quantitative. We thus anticipate widespread use of HARPES in the future, with many materials being amenable to study in the 1–3 keV regime[13], and better theory and data-analysis procedures likely to push this to energies as high as 5–10 keV.

Methods

Our HARPES experiments were carried out at the synchrotron radiation facility SPring-8 in Hyogo, Japan, using undulator beamline BL15XU (ref. 34). The samples of W and GaAs were highly polished, but not subjected to any special cleaning. The photoemitted electrons were detected and analysed for their kinetic energy using a VG Scienta R4000 hemispherical analyser, set in angle-resolving mode. The overall energy resolution (monochromator plus analyser) was set to 250 meV, as verified by measuring the spectra of the Au valence band at the Fermi level. The angular resolution in one direction of the two-dimensional detector image is about 0.25°–0.30°, as judged by an extensive set of ray tracings (B. Wannberg, private communication). The X-ray incidence angle, as measured from the sample surface, was fixed at 2° for W and 1° for GaAs. The angle between the electron spectrometer lens axis and photon propagation was fixed at 90°, resulting in electron take-off angles of 88° for W and 89° for GaAs, as measured from the sample surface. The geometries are illustrated in Figs 1f and 2f. The photons were p-polarized, that is, the electric field vector was in the plane of incidence and always pointing in the direction of the electron detector. The sample manipulator allowed the sample to be cooled by liquid helium down to 20–30 K. For both samples, measurements were made at room temperature and 20–30 K.

Received 25 November 2010; accepted 5 July 2011; published online 14 August 2011

References

1. Himpsel, F. J. Angle-resolved measurements of the photoemission of electrons in the study of solids. *Adv. Phys.* **32,** 1–51 (1983).
2. Hüfner, S. *Photoelectron Spectroscopy: Principles and Applications* 2nd edn (Springer, 1996).
3. Damascelli, A., Hussain, Z. & Shen, Z-X. Angle-resolved photoemission studies of the cuprate superconductors. *Rev. Mod. Phys.* **75,** 473–541 (2003).
4. Christensen, N. E. & Feuerbacher, B. Volume and surface photoemission from tungsten. I. Calculation of band structure and emission spectra. *Phys. Rev. B* **10,** 2349–2372 (1974).
5. Feydt, J., Elbe, A., Engelhard, H. & Meister, G. Photoemission from bulk bands along the surface normal of W(110). *Phys. Rev. B* **58,** 14007–14012 (1998).
6. Hussain, Z., Fadley, C. S., Kono, S. & Wagner, L. F. Temperature-dependent angle-resolved X-ray photoemission study of the valence bands of single-crystal

tungsten: Evidence for direct transitions and phonon effects. *Phys. Rev. B* **22,** 3750–3766 (1980).
7. Emtsev, K. V., Speck, F., Seyller, T. & Ley, L. Interaction, growth, and ordering of epitaxial graphene on SiC{0001} surfaces: A comparative photoelectron spectroscopy study. *Phys. Rev. B* **77,** 155303 (2008).
8. Ando, T., Fowler, A. B. & Stern, F. Electronic properties of two-dimensional systems. *Rev. Mod. Phys.* **54,** 437–672 (1982).
9. Tamai, A. *et al.* Fermi surface and van Hove singularities in the itinerant metamagnet $Sr_3Ru_2O_7$. *Phys. Rev. Lett.* **101,** 026407 (2008).
10. Claesson, T. *et al.* Angle resolved photoemission from $Nd_{1.85}Ce_{0.15}CuO_4$ using high energy photons: A Fermi surface investigation. *Phys. Rev. Lett.* **93,** 136402 (2004).
11. Venturini, F., Minár, J., Braun, J., Ebert, H. & Brookes, N. B. Soft x-ray angle-resolved photoemission spectroscopy on Ag(001): Band mapping, photon momentum effects, and circular dichroism. *Phys. Rev. B* **77,** 045126 (2008).
12. Plucinski, L. *et al.* Band mapping in higher-energy x-ray photoemission: Phonon effects and comparison to one-step theory. *Phys. Rev. B* **78,** 035108 (2008).
13. Papp, C. *et al.* Band mapping in x-ray photoelectron spectroscopy: An experimental and theoretical study of W(110) with 1.25 keV excitation. *Phys. Rev. B* **84,** 045433 (2011).
14. Fadley, C. S. X-ray photoelectron spectroscopy and diffraction in the hard X-ray regime: Fundamental considerations and future possibilities. *Nucl. Instrum. Methods Phys. Res. A* **547,** 24–41 (2005).
15. Kobayashi, K. High-resolution hard X-ray photoelectron spectroscopy: Application of valence band and core-level spectroscopy to materials science. *Nucl. Instrum. Methods Phys. Res. A* **547,** 98–112 (2005).
16. Tanuma, S., Powell, C. J. & Penn, D. R. Calculations of electron inelastic mean free paths. *Surf. Interface Anal.* **37,** 1–14 (2005).
17. Tanuma, S. *et al.* Experimental determination of electron inelastic mean free paths in 13 elemental solids in the 50 to 5000 eV energy range by elastic-peak electron spectroscopy. *Surf. Interface Anal.* **37,** 833–845 (2005).
18. Tanuma, S., Powell, C. J. & Penn, D. R. Calculations of electron inelastic mean free paths. IX. Data for 41 elemental solids over the 50 eV to 30 keV range. *Surf. Interface Anal.* **43,** 689–713 (2011).
19. Shevchik, N. J. Disorder effects in angle-resolved photoelectron spectroscopy. *Phys. Rev. B* **16,** 3428–3442 (1977).
20. Takata, Y. *et al.* Recoil effect of photoelectrons in the Fermi edge of simple metals. *Phys. Rev. Lett.* **101,** 137601 (2008).
21. Feuerbacher, B. & Christensen, N. E. Volume and surface photoemission from tungsten. II. Experiment. *Phys. Rev. B* **10,** 2373–2390 (1974).
22. Hussain, Z., Umbach, E., Barton, J. J., Tobin, J. G. & Shirley, D. A. Angle-resolved photoemission study of the valence bands of W(011) in the photon energy range 1100–1250 eV: Observation of strong direct transitions and phonon effects. *Phys. Rev. B* **25,** 672–676 (1982).
23. Ieong, M., Doris, B., Kedzierski, J., Rim, K. & Yang, M. Silicon device scaling to the sub-10-nm regime. *Science* **306,** 2057–2060 (2004).
24. Chau, R. *et al.* Benchmarking nanotechnology for high-performance and low-power logic transistor applications. *IEEE Trans. Nanotech.* **4,** 153–158 (2005).
25. Brammertz, G. *et al.* GaAs on Ge for CMOS. *Thin Solid Films* **517,** 148–151 (2008).
26. Ye, P. D. *et al.* GaAs metal–oxide–semiconductor field-effect transistor with nanometer-thin dielectric grown by atomic layer deposition. *Appl. Phys. Lett.* **83,** 180–182 (2003).
27. Wu, J. D., Huang, Y. S., Brammertz, G. & Tiong, K. K. Optical characterization of thin epitaxial GaAs films on Ge substrates. *J. Appl. Phys.* **106,** 023505 (2009).
28. Zhu, H. J. *et al.* Room-temperature spin injection from Fe into GaAs. *Phys. Rev. Lett.* **87,** 016601 (2001).
29. Dallera, C. *et al.* Looking 100 Å deep into spatially inhomogeneous dilute systems with hard X-ray photoemission. *Appl. Phys. Lett.* **85,** 4532 (2004).
30. Alvarez, M. A. V., Ascolani, H. & Zampieri, G. Excitation of phonons and forward focusing in X-ray photoemission from the valence band. *Phys. Rev. B* **54,** 14703–14712 (1996).
31. Blaha, P., Schwarz, K., Madsen, G., Kvasnicka, D. & Luitz, J. *WIEN2k, an Augmented Plane Wave + Local Orbitals Program for Calculating Crystal Properties* (Karlheinz Schwarz, Techn. Universit. Wien, 2001).
32. Braun, J., Minár, J., Ebert, H., Katsnelson, M. I. & Lichtenstein, A. I. Spectral function of ferromagnetic 3d metals: A self-consistent LSDA+DMFT approach combined with the one-step model of photoemission. *Phys. Rev. Lett.* **97,** 227601 (2006).
33. Bachelet, G. B. & Christensen, N. E. Relativistic and core-relaxation effects on the energy bands of gallium arsenide and germanium. *Phys. Rev. B* **31,** 879–887 (1985).
34. Ueda, S. *et al.* Present status of the NIMS contract beamline BL15XU at SPring-8. *AIP Conf. Proc.* **1234,** 403–406 (2010).

Acknowledgements

The authors would like to thank O. D. Dubon (UC Berkeley) for providing the GaAs sample. The authors with LBNL affiliation acknowledge support from the Director, Office of Science, Office of Basic Energy Sciences, Materials Sciences and Engineering Division, of the US Department of Energy under contract number DE-AC02-05CH11231, for salary and travel support. The measurements were performed under the approval of NIMS Beamline Station (Proposal Nos. 2008A4906, 2008B4800, 2009A4906). This work was partially supported by the Nanotechnology Network Project, the Ministry of Education, Culture, Sports, Science and Technology (MEXT), Japan. Financial support by the Deutsche Forschungsgemeinschaft (FOR 1346, EB-154/20 and MI-1327/1) and the Bundesministerium für Bildung und Forschung (05K10WMA) is also gratefully acknowledged.

Author contributions

A.X.G., C.P., S.U. and B.B. carried out the experiments, with assistance from Y.Y. and under the supervision of K.K. and C.S.F. Data normalization and analysis were performed by C.P. and A.X.G. Free-electron final-state model calculations were performed by L.P., with assistance from C.M.S. One-step model calculations were performed by J.M., J.B. and H.E. DFT calculations were performed by E.R.Y. and W.E.P.

Additional information

The authors declare no competing financial interests. Supplementary information accompanies this paper on www.nature.com/naturematerials. Reprints and permissions information is available online at http://www.nature.com/reprints. Correspondence and requests for materials should be addressed to A.X.G.